Facile synthesis of novel ultrathin α-MoO_3 square nanosheets with excellent adsorptive capacity and photocatalytic performance for efficient treatment of Rhodamine B

Guogang Tang[1] ✉, *Feixia Zhang*[1], *Jing Xu*[2] ✉

[1]*Zhenjiang College, Zhenjiang, Jiangsu province 212003, People's Republic of China*
[2]*School of Materials Science and Engineering, Jiangsu University, Zhenjiang, Jiangsu province 212013, People's Republic of China*
✉ *E-mail: g_tang78@hotmail.com, xjing@ujs.edu.cn*

Published in Micro & Nano Letters; Received on 22nd July 2018; Revised on 9th November 2018; Accepted on 12th December 2018

Novel ultrathin α-MoO_3 square nanosheets with the width of 200–400 nm and the thickness of ~50 nm were synthesised successfully via a facile and efficient solid sintered method using the carbon@MoS_2 nanocomposites as precursor. The as-prepared products were characterised by X-ray powder diffraction, scanning electron microscopy, transmission electron microscopy, and tested in adsorption and photocatalysis to remove Rhodamine B (RhB). Compared with commercial MoO_3 and/or MoO_3 nanorods, α-MoO_3 square nanosheets exhibit greater adsorptive capacity and photocatalytic performance for degrading RhB. Moreover, this combination of adsorption and photocatalysis using α-MoO_3 could be promising is demonstrated as a more pressing technique for contaminant removal from wastewater.

1. Introduction: In the past decades, with the development of global industrialisation and the process of urbanisation, wastewater contaminated by organic pollutant and/or toxicity has become one of the most urgent environmental problems. Compared with many traditional techniques, semiconductor photocatalysis, as a novel and 'green' strategy, offers a tempting prospect and attracts considerable attention for clean energy and environmental remediation [1–3]. Moreover, adsorption/photocatalysis has been considered as a promising and efficient method to remove organic pollutant from aqueous solutions due to low cost, convenient operation, flexibility, small amounts of harmful substances and simple design. Interestingly, many recent reports also indicate superior adsorption of semiconductor is contributed to enhance their photocatalytic activity [4, 5]. For this reason, seeking and synthesis of the visible-light-driven photocatalysts with higher adsorption and photocatalytic efficiency for the degradation of organic pollutants has become the most pressing environmental problems in the current wastewater purification field.

In recent years, with the rise of graphene, two-dimensional (2D) materials have been attracted extensive attention and show intriguing electronic, electrocatalytic, photocatalytic and adsorption properties [6–10]. Moreover, many previous works also indicate graphene-like materials can easily adsorb more organic contaminants from aqueous solution due to their larger specific surface areas and characteristic laminated structure. So far amongst 2D materials, Mo-based compounds such as MoS_2, $MoSe_2$, MoO_3 and so on, is believed to have potential for organic contaminant degradation and solving energy problems owing to their unique layered structure and excellent absorption. Among the above Mo-based photocatalysts, MoO_3 is one of the most fascinating star semiconductor due to its rich chemistry associated with multiple valence states, high chemical stability and abundant in source [11–16]. Generally, MoO_3 exists in three kinds of crystal structures: orthorhombic α-MoO_3, monoclinic β-MoO_3 and hexagonal MoO_3. Orthorhombic a-MoO_3 phase has unique layered structure forming by corner-sharing [MoO_6] octahedrons along the [001] and [100] directions, which can be selected as a photocatalysis to fabricate anisotropic nanostructures with superior properties in photocatalytic applications [14–16]. Very recently, many α-MoO_3 with special morphologies including nanorods, nanowires, nanobelts and nanoplates were synthesised and shown excellent photocatalytic activity for degrading organic pollutants [17–20]. Therefore, the modification of the structural and optical properties of MoO_3 with controlled morphology is a promising and challenging task for photodegradation of organic pollutants.

Herein, we first report the synthesis of ultrathin α-MoO_3 square nanosheets by a facile and efficient solid sintered method using the carbon@MoS_2 nanocomposites as precursor. The adsorption and photocatalytic performance of α-MoO_3 square nanosheets have been studied by the degradation of Rhodamine B (RhB), which exhibit greater adsorptive capacity and photocatalytic performance. More importantly, our researchers will provide new insights into designing Mo-based photocatalyst with high adsorption/photocatalysis performance for realising a revolution of clean and renewable energy.

2. Experimental section

2.1. Catalysts preparation

2.1.1. Synthesis of resorcinol–formaldehyde (RF) resin spheres: All chemical reagents were of analytic purity from the Sinopharm Chemical Reagent Co., Ltd. and used directly without further purification.

The monodisperse RF resins spheres were synthesised by using resorcinol and formaldehyde solution as precursors [21]. In a typical synthesis of e RF resins spheres, ammonia aqueous solution (NH_4OH, 0.1 ml, 25 wt%) was mixed with a solution containing absolute ethanol (EtOH, 8 ml) and deionised water (H_2O, 20 ml), then stirred for >1 h. Subsequently, resorcinol (0.2 g) was added and continually stirred for 0.5 h. The formaldehyde solution (0.28 ml) then added to the reaction solution and stirred for 24 h at 30°C, and subsequently heated for 24 h at 100°C under a static condition in a Teflon-lined autoclave. The solid product was recovered by centrifugation and air-dried at 80°C for 48 h.

2.1.2. Synthesis of carbon@MoS_2 precursors: The carbon@MoS_2 nanocomposites were synthesised by a hydrothermal process and as follows: as-prepared RF resins spheres (0.01 g) were dissolved in 60 ml deionised water, then 0.44 g of Na_2MoO_4, 0.35 g $NH_2OH \bullet HCl$ and 0.60 g of Na_2S were added to the solution under constant stirring. Moreover, pH value of the mixture was

doi: 10.1049/mnl.2018.5420

adjusted to 6 by the addition of 2 mol/l HCl. The mixture was then transferred into a 100 ml Teflon-lined stainless steel autoclave and sealed, and the autoclave was placed in a pre-heated oven at 180°C for 24 h and naturally cooled down to room temperature. Black precipitates were collected by centrifugation and washed with distilled water and absolute ethanol for several times, and finally dried in vacuum at 80°C for 8 h.

2.1.3. Synthesis of α-MoO_3 square nanosheets: The α-MoO_3 square nanosheets were prepared by a solid sintered approach using the above carbon@MoS_2 as a precursor. Typically, carbon@MoS_2 precursors were transferred into a temperature-controlled tube furnace, and heated to 450°C in an air atmosphere for 4 h to remove the carbon template and transform into α-MoO_3. After that, the reactor is gradually cooled to room and a black powder is obtained. In addition, commercial MoO_3 was also of analytic purity from the Sinopharm Chemical Reagent Co., Ltd. And MoO_3 nanorods were synthesised by a simple hydrothermal process according to a reported procedure [18].

2.2. Characterisation: The X-ray diffraction patterns were recorded using a D8 advance (Bruker-AXS) diffractometer with Cu *Ka* radiation ($\lambda = 0.1546$ nm). The morphology of the sample was observed on a scanning electron microscope (SEM, JEOL JXA-840A) with an acceleration voltage of 15 kV. Transmission electron microscopic (TEM) images were further characterised the morphology of the as-prepared products using a Japan JEM-100CX II transmission electron microscopy operated at an accelerating voltage of 100 kV.

2.3. Photocatalytic test: In our experiment, RhB was chosen as the simulated pollutants to evaluate the adsorption and photocatalytic performance of the as-prepared MoO_3 catalysts. In a typical adsorption experiment, 25 mg of adsorbent was added to a series of 250 ml beakers with RhB solutions (100 ml, 10–40 mg/l) under constant stirring in dark. During the adsorption period, 2 ml of suspension was removed from the reactor at regular time intervals of 10 min and centrifuged. Finally, the concentration of RhB was analysed by the Lambda 25UV/vis spectrophotometer.

Similarly, the photocatalytic experimental process is as follow: 25 mg of photocatalyst was added to a low-acidity aqueous solution containing 200 ml of RhB aqueous solution (20 mg/l) and was magnetically stirred in the dark for 0.5 h under continuous stirring to establish equilibrium between the dye and the catalyst. At a given time (30 min) interval after commencement of irradiation, about 5 ml suspensions were collected and centrifuged (10,000 rpm, 5 min) to remove the photocatalyst particles. The supernatants were collected and analysed by recording variations of the absorption band maximum in the UV–vis spectra by using a Lambda 25UV/vis spectrophotometer. Moreover, photocatalytic activity of commercial MoO_3 and MoO_3 nanorods were also measured for comparison.

3. Results and discussion: Novel ultrathin α-MoO_3 square nanosheets were synthesised by a facile and efficient two-step chemical reaction, as schematically shown in Fig. 1. Firstly, carbon@MoS_2 nanocomposites were prepared by a hydrothermal process using carbon nanospheres as templates in aqueous solution. Secondly, α-MoO_3 square nanosheets were prepared by a solid sintered approach using the above carbon@MoS_2 as a precursor. Carbon nanospheres play a significant role in the shape-controlled synthesis of the final products due to its steric effect. Based on the above analysis, the reactions of MoO_3 can be expressed as follows:

$$Na_2MoO_4 + 4Na_2S + 4H_2O \rightarrow Na_2MoS_4 + 8NH_3 + 4CO_2 \quad (1)$$

$$Na_2MoS_4 + 2NH_2OH \cdot HCl \rightarrow MoS_2 + N_2 + 2H_2O + 2H_2S \quad (2)$$

$$2MoS_2 + 3O_2 \rightarrow 2MoO_3 + 2SO_2 \quad (3)$$

The crystal phase of carbon@MoS_2 composites and α-MoO_3 nanosheets was confirmed by X-ray diffraction analysis and resulted in Fig. 2. Clearly, all the diffraction peaks of the obtained carbon@MoS_2 composites can be assigned to hexagonal MoS_2 (JCPDS Card No. 37-1492), and no other impurity peaks were indexed in the XRD pattern. Moreover, typical patterns of carbon in carbon@MoS_2 composites could not be observable due to its low content and poor crystalline structures. After calcination, all XRD patterns of α-MoO_3 nanosheets could be indexed to orthorhombic phase of α-MoO_3 (JCPDS card No. 35-0609). Moreover, the crystallisation processes of α-MoO_3 were examined by thermal analyses of the dried samples at temperature ranges of 30–600°C, as shown Fig. 3. Clearly, no obvious mass loss is observed up to 600°C for prepared MoO_3 nanobelts, indicating that the bare MoO_3 remains stable over the entire temperature

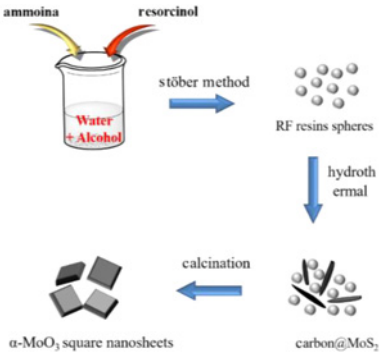

Fig. 1 *Schematic illustration of the synthesis of α-MoO_3 square nanosheets*

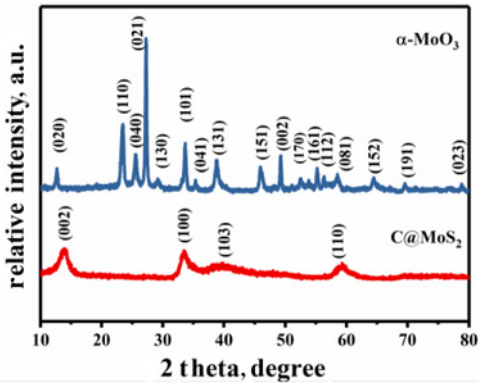

Fig. 2 *XRD patterns of carbon@MoS_2 and α-MoO_3 square nanosheets*

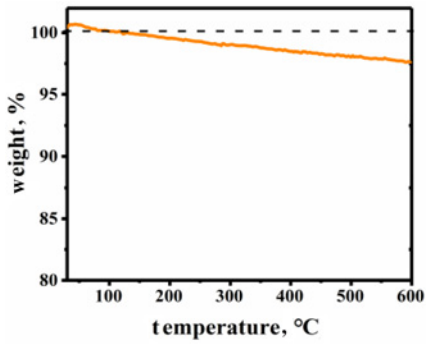

Fig. 3 *Thermal analyses of the as-prepared α-MoO_3 square nanosheets*

range. And the slight mass loss (0.70%) is caused by the loss of the absorbed water on the surface of the as-prepared a-MoO_3, which well agreed with XRD results.

The surface morphology and structure of carbon nanospheres, carbon@MoS_2 composites and α-MoO_3 nanosheets were carried out by SEM and TEM. As can be seen from Figs. 4*a* and *b*, carbon nanospheres with the average diameters of 100–200 nm were observed by an extension of the Stöber method. Figs. 4*c* and *d* show petal-like MoS_2 nanosheets evenly coated carbon nanospheres through a hydrothermal process. After removal of carbon nanospheres templates by calcination at 450°C, ultrathin α-MoO_3 square nanosheets with the width of 200–400 nm and the thickness of ~50 nm can be synthesised (Fig. 4*e*), which indicated steric effect of carbon nanospheres is help for the morphological control of α-MoO_3. Further characterisation of α-MoO_3 nanosheets was performed by HRTEM (Fig. 4*f*), clear Parallel lattice fringes with interplanar spacing of about 0.327 nm can be observed, corresponding to (0 2 1) crystal planes of theorthorhombic phase of α-MoO_3, which is consistent with the calculated spacing from XRD patterns. Moreover, the SAED pattern of sample (inset of Fig. 5*c*) indicates α-MoO_3 nanosheets are single crystalline with the top/bottom surface of [0 1 0] and the growth lying preferentially along the [0 2 1] direction.

To evaluate the potential application in water treatment of as-prepared α-MoO_3 square nanosheets, the adsorption capacities for RhB in the absence of light irradiation, are investigated. Obviously, α-MoO_3 square nanosheets exhibited higher adsorption ability compared with commercial MoO_3, MoO_3 nanorods and MoS_2 nanoflowers, as shown in Fig. 5*a*. Moreover, ~80% of RhB was removed by adsorption for α-MoO_3 square nanosheets within 18 min, and after that the above adsorption process quickly reaches an adsorption/desorption equilibrium. Fig. 5*b* shows the adsorption curves measured with different concentrations of 10–30 mg/l using α-MoO_3 square nanosheets as adsorbents. When RhB concentrations increase to 10 and 30 mg/l, the adsorption rates were extraordinarily fast in the first 20 min under all concentrations. Then after 20 min a long period of slower uptake was followed, and finally adsorbed amount reached its equilibrium. More importantly, the removal rate of α-MoO_3 square nanosheets remains almost the same and the maximum removal rate reaches to 98.1% at MB concentration of 10 mg/l and 88.2% at MB concentration of 30 mg/l after adsorption for 30 min. In addition, the photocatalytic activities of the above as-prepared products were evaluated for the photodegradation of RhB aqueous solution (20 mg/l) under visible light exposure after adsorption equilibrium

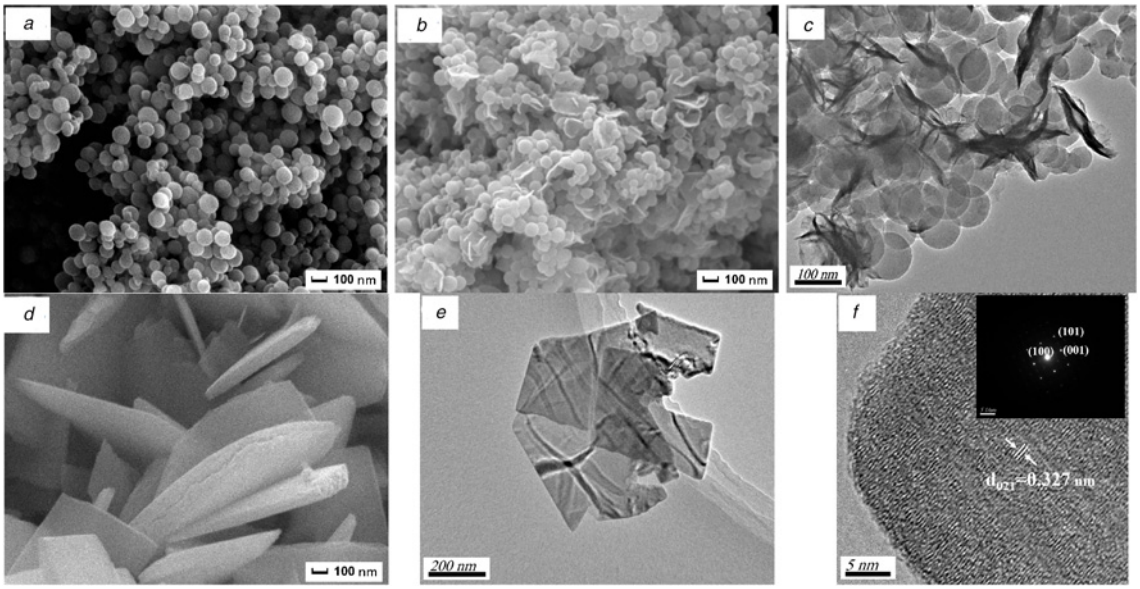

Fig. 4 *SEM and TEM image of*
a RF resins spheres
b, *c* Carbon@MoS_2 and
d, *e* α-MoO_3 square nanosheets
f HRTEM image and SAED pattern (inset) of α-MoO_3 square nanosheets

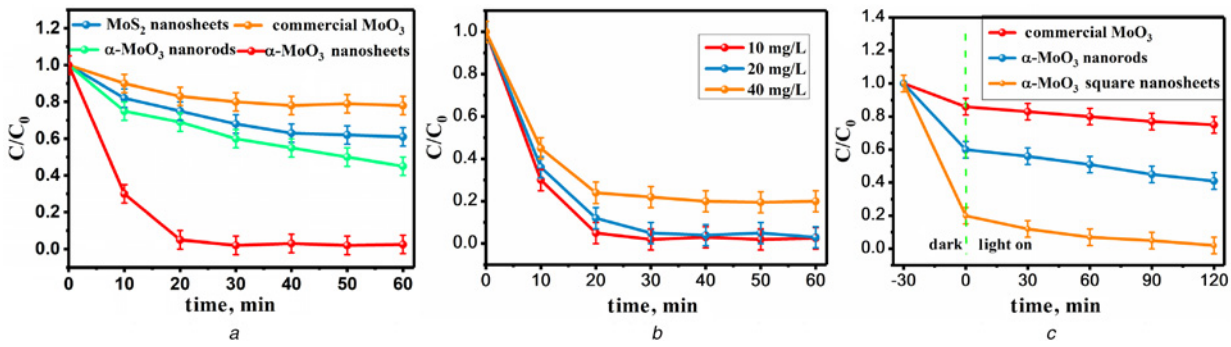

Fig. 5 *Absorption rate and Photocatalytic activity of RhB in the presence of different samples*
a Time-dependent absorption rate of RhB in the presence of different samples
b Change in initial concentration of RhB in the presence of α-MoO_3 square nanosheets
c Photocatalytic activity of different photocatalysts in the decomposition of RhB (20 mg/l); and the above experiments were repeated three times

doi: 10.1049/mnl.2018.5420

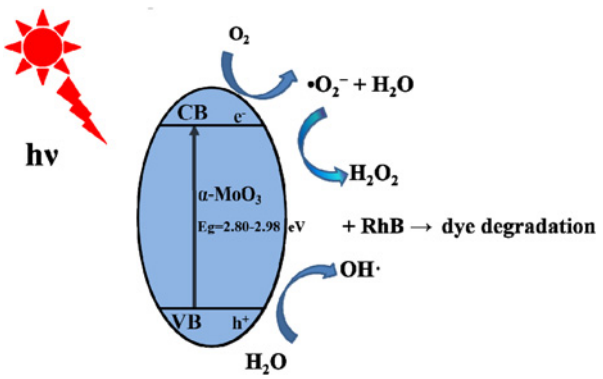

Fig. 6 *Schematic representation of reactive radical formation in α-MoO_3 square nanosheets under visible light and photodegradation of dyes*

for 30 min. It can be seen from Fig. 5*c* that α-MoO_3 square nanosheets showed higher photocatalytic decolourisation of RhB than commercial MoO_3 and MoO_3 nanorods. When using commercial MoO_3 as a photocatalyst, only 24% of RhB are degraded in 60 min. On the contrary, the degradation efficiency of of RhB over α-MoO_3 square nanosheets and MoO_3 nanorods is 86 and 95% in the same time, respectively. The above experimental results also indicated sheets-like structures and excellent adsorption is beneficial for enhancing the efficiency of photocatalyst.

As is well known, photocatalytic activity is affected by many factors which could influence each other and enhance the photocatalytic ability [20–22]. Many previous reports also indicate faster and complete degradation of dyes under visible light irradiation is attributed to the optical band gap of α-MoO_3 (2.80–2.98 eV) that lies in the visible region and promotes stronger absorption of photons. Based on the above experimental results and the related literature reports, the photodegradation mechanism is schematically shown in Fig. 6. In the photocatalytic process, the absorption of photons by α-MoO_3 nanosheets generates charge carrier that diffuse to the surface of nanoparticles under visible light excitation. Meanwhile, the reaction photo-excited electrons with oxygen produced superoxide radicals ($\bullet O^{2-}$) and reaction holes with water lead to the formation of hydroxyl radicals ($\bullet$OH), which are two crucial reactive radicals and responsible for the degradation of pollutant. However, the exact adsorption and photocatalytic mechanism of α-MoO_3 square nanosheets can be further developed.

4. Conclusion: In summary, novel ultrathin α-MoO_3 square nanosheets were synthesised successfully via a facile and efficient solid sintered method using the carbon@MoS_2 nanocomposites as precursor. Subsequently, α-MoO_3 square nanosheets exhibited excellent adsorptive capacity and photocatalytic performance for degrading RhB compared to that of commercial MoO_3 and/or MoO_3 nanorods, which could be promising materials in the field of photocatalysis, wastewater treatment and environmental remediation. More importantly, 2D structures and excellent adsorption of α-MoO_3 played fundamental roles in enhancing its photocatalytic activity. Furthermore, our controllable synthesis route can provide unprecedented insights for the development of metal oxide semiconductor with 2D structures for various potential applications, such as pollutant purification, lithium battery, photochromic and optical devices.

5. Acknowledgments: This work was financially supported by the China Postdoctoral Science Foundation (grant nos. 2017M611733 and 2017M611715), Natural Science Foundation of Jiangsu Higher Education Institutions of China (grant no. 17KJB30012), High-end Research Project of Jiangsu Higher Vocational Education Institutions (grant no. 2018TDFX010) and Primary Research & Development Plan (social development project) of Zhenjiang (grant no.SH2017059), Dr. G. Tang gratefully acknowledges financial support from the second batch of scientific research team of Zhenjiang College.

6 References

[1] Zhao L., Deng J., Sun P., *ET AL.*: 'Nanomaterials for treating emerging contaminants in water by adsorption and photocatalysis: systematic review and bibliometric analysis', *Sci. Total Environ.*, 2018, **627**, pp. 1253–1263
[2] Boyjoo Y., Sun H., Liu J., *ET AL.*: 'A review on photocatalysis for air treatment: from catalyst development to reactor design', *Chem. Eng. J.*, 2017, **310**, pp. 537–559
[3] Li Z., Meng X., Zhang Z., *ET AL.*: 'Recent development on Mo_{S2}-based photocatalysis: a review', *J. Photochem. Photobiol. C, Photochem. Rev.*, 2018, **35**, pp. 39–55
[4] Akinwande D., Brennan C. J., Bunch J.S., *ET AL.*: 'A review on mechanics and mechanical properties of 2D materials–graphene and beyond', *Extreme. Mech. Lett.*, 2017, **13**, pp. 42–77
[5] Cui Z., Sun Y.: 'From tremella-like MoS_2 to α-MoO_3 nanoplates: sintering synthesis and adsorption properties', *Micro Nano Lett.*, 2017, **12**, pp. 652–655
[6] Tang G.G., Sun J.C., Wei C., *ET AL.*: 'Synthesis and characterization of flowerlike MoS2 nanostructures through CTAB-assisted hydrothermal process', *Mater. Lett.*, 2012, **86**, pp. 9–12
[7] Lu X., Utama M. I. B., Lin J., *ET AL.*: 'Large-area synthesis of monolayer and few-layer MoSe2 films on SiO_2 substrates', *Nano Lett.*, 2014, **14**, (5), pp. 2419–2425
[8] Shaw J. C., Zhou H., Chen Y., *ET AL.*: 'Chemical vapor deposition growth of monolayer $MoSe_2$ nanosheets', *Nano Res.*, 2014, **7**, (4), pp. 511–517
[9] Tang G., Zhang J., Liu C., *ET AL.*: 'Synthesis and tribological properties of flower-like MoS_2 microspheres', *Ceram. Int.*, 2014, **40**, (8), pp. 11575–11580
[10] Mai L. Q., Hu B., Chen W., *ET AL.*: 'Lithiated MoO_3 nanobelts with greatly improved performance for lithium batteries. *Adv. Mater.*, 2007, **19**, (21), pp. 3712–3716
[11] Sheehan P. E., Lieber C.: 'Nanotribology and nanofabrication of MoO_3 structures by atomic force microscopy', *Science*, 1996, **272**, (5265), pp. 1158–1161
[12] Zhou K., Zhou W., Liu X., *ET AL.*: 'Ultrathin MoO_3 nanocrystals self-assembled on graphene nanosheets via oxygen bonding as supercapacitor electrodes of high capacitance and long cycle life', *Nano Energy*, 2015, **12**, pp. 510–520
[13] Ahmed B., Shahid M., Nagaraju D.H., *ET AL.*: 'Surface passivation of MoO_3 nanorods by atomic layer deposition toward high rate durable Li ion battery anodes', *ACS Appl. Mater. Interfaces*, 2015, **7**, (24), pp. 13154–13163
[14] Zhang Q., Lv J. N., Hu X. Y., *ET AL.*: 'Polyaniline decorated MoO_3 nanorods: synthesis, characterization and promoting effect to Pt electrocatalyst', *Int. J. Hydrog. Energy*, 2018, **43**, (11), pp. 5603–5609
[15] Manivel A., Lee G. J., Chen C.Y., *ET AL.*: 'Synthesis of MoO_3 nanoparticles for AZO dye degradation by catalytic ozonation', *Mater. Res. Bull.*, 2015, **62**, pp. 184–191
[16] Arfaoui A., Touihri S., Mhamdi A., *ET AL.*: 'Structural, morphological, gas sensing and photocatalytic characterization of MoO_3 and WO_3 thin films prepared by the thermal vacuum evaporation technique', *Appl. Surf. Sci.*, 2015, **357**, pp. 1089–1096
[17] Kumar V. V., Gayathri K., Anthony S.P.: 'Synthesis of α-MoO_3 nanoplates using organic aliphatic acids and investigation of sunlight enhanced photodegradation of organic dyes', *Mater. Res. Bull.*, 2016, **76**, pp. 147–154
[18] Ghaffar I., Warsi M. F., Shahid M., *ET AL.*: 'Unprecedented photocatalytic activity of carbon coated/MoO_3 core–shell nanoheterostructurs under visible light irradiation', *Physica E*, 2016, **79**, pp. 1–7
[19] Hu H., Deng C., Xu J., *ET AL.*: 'Metastable h-MoO_3 and stable α-MoO_3 microstructures: controllable synthesis, growth mechanism and their enhanced photocatalytic activity', *J. Exp. Nanosci.*, 2015, **10**, (17), pp. 1336–1346
[20] Ma Y., Jia Y.L., Jiao Z.B., *ET AL.*: 'Facile synthesize α-MoO_3 nanobelts with high adsorption property', *Mater. Lett.*, 2015, **157**, pp. 53–56
[21] Liu J., Qiao S.Z., Liu H., *ET AL.*: 'Extension of the Stöber method to the preparation of monodisperse resorcinol–formaldehyde resin polymer and carbon spheres', *Angew. Chem.*, 2011, **123**, pp. 6069–6073
[22] Xu D., Bai Y., Li Z., *ET AL.*: 'Enhanced photodegradation ability of solvothermally synthesized metallic copper coated ZnO microrods', *Colloids Surf. A: Physicochem. Eng. Aspects* 2018, **548**, pp. 19–26